Solar Energy Materials & Solar Cells 130 (2014) 474–480

Contents lists available at ScienceDirect

Solar Energy Materials & Solar Cells

journal homepage: www.elsevier.com/locate/solmat

Inkjet printing processing conditions for bulk-heterojunction solar cells using two high-performing conjugated polymer donors

Felix Hermerschmidt [a], Paris Papagiorgis [b], Achilleas Savva [a], Constantinos Christodoulou [a], Grigorios Itskos [b], Stelios A. Choulis [a,*]

[a] Molecular Electronics and Photonics Research Unit, Department of Mechanical Engineering and Materials Science and Engineering, Cyprus University of Technology, 3041 Limassol, Cyprus
[b] Department of Physics, Experimental Condensed Matter Physics Laboratory, University of Cyprus, 1678 Nicosia, Cyprus

ARTICLE INFO

Article history:
Received 5 May 2014
Received in revised form
25 July 2014
Accepted 31 July 2014

Keywords:
Printed electronics
Organic photovoltaics
Inkjet printing and processing
Conjugated polymers
Morphology

ABSTRACT

We report the processing conditions for inkjet-printed active layers of organic photovoltaic (OPV) devices comprising bulk-heterojunction blends of the low bandgap conjugated polymer poly[(4,4′-bis(2-ethylhexyl) dithieno[3,2-b:2′,3′-d]silole)-2,6-diyl-*alt*-(4,7-bis(2-thienyl)-2,1,3-benzothiadiazole)-5,5′-diyl] (Si-PCPDTBT) as well as poly[*N*-9′-hepta-decanyl-2,7-carbazole-alt-5,5-(4′,7′-di-2-thienyl-2′,1′,3′-benzothiadiazole)] (PCDTBT) used as electron donors with [6,6]-phenyl-C71-butyric acid methyl ester ($PC_{70}BM$) as electron acceptor. By controlling the inkjet printing processing conditions, we gain a significant improvement in device power conversion efficiency (PCE) to previously reported work using these materials. We obtain Si-PCPDTBT:fullerene and PCDTBT:fullerene-based inkjet-printed OPVs with power conversion efficiency of ~3% and ~4%, respectively.

1. Introduction

In the last decade the interest in renewable energy sources has grown rapidly. The sun plays a crucial role as its incident light on Earth provides an abundant source of energy—the amount striking Earth in less than an hour is sufficient to satisfy the average yearly human consumption [1]. The research community has therefore been focused on harnessing this energy with the aim of providing a stable and renewable method of producing electricity. OPVs can contribute to this need for sustainable energy resources by providing a low-cost, solution-processable and environmentally friendly alternative.

Bulk-heterojunction (BHJ) devices are proving especially worthwhile candidates, most commonly making use of an electron donating conjugated polymer and an electron accepting fullerene unit to provide a flow of electrons to the electrodes. OPV BHJ devices are now reaching a power conversion efficiency (PCE) above certified 8% [2]; with even above 10% being reported [3].

One of the fundamental concerns for organic photovoltaics (OPVs) is compatibility with printing manufacturing. Only then can OPV commercialization be truly viable [4]. One such compatible technique is inkjet-printing. Its drop-on-demand (DoD) technology allows the ink droplets to be deposited exactly where required on the substrate [5]. This technique demands specific processing parameters in order to achieve morphology control similar to OPV device fabricated with common lab-scale techniques, such as doctor blading or spin coating [6–9].

An inkjet printer can also be seamlessly integrated into a roll-to-roll (R2R) production process, which can produce a large throughput of cells or large area devices [10]. Inkjet printing has been used to manufacture all the main components of an OPV device—from the metal electrodes to transparent conductive materials and also the active layers. The processes used for each of these components differ greatly and competing techniques exist with regard to high throughput, degree of accuracy, material consumption and energy payback [11]. Inkjet printing mainly competes with screen printing or flexographic printing for R2R compatible deposition of the metal electrodes, such as a transparent grid structure to replace ITO or a bulk metal structure as a back electrode [12,13]. For high throughput active layer deposition slot-die coating may be viewed as preferable, however, inkjet printing is still advantageous with regard to low material consumption and flexibility because of its DoD properties.

Due to the fact that the intricate network of conjugated polymer donor and acceptor morphology within a BHJ blend determines the performance of an organic solar cell, it is important to preserve this intricate morphology when producing thin films from a liquid solution. It is therefore imperative to gain knowledge

* Corresponding author.
E-mail address: stelios.choulis@cut.ac.cy (S.A. Choulis).

http://dx.doi.org/10.1016/j.solmat.2014.07.050
0927-0248/

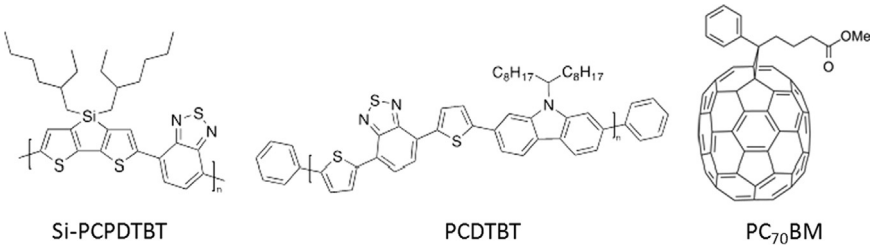

Fig. 1. Chemical structures of materials used in this study.

on desired inkjet-printing parameters to further improve obtained device performance [14]. The potential of combining inkjet-printed active layers with other inkjet-printed components of the OPV device, such as the bottom electrode currently mostly comprised of expensive indium tin oxide [15,16], can pave the way for highly efficient fully inkjet-printed devices.

To date, good inkjet-printed solar cells with a power conversion efficiency of approx. 3–4% have been achieved using active layer blends of the well-known poly(3-hexylthiophene) (P3HT) and phenyl-C71-butyric acid methyl ester ($PC_{70}BM$) [17–21]. However, high performing conjugated polymers have so far not been widely included in inkjet studies. One of these high performing conjugated polymers is poly[(4,4′-bis(2-ethylhexyl)dithieno[3,2-b:2′,3′-d]silole)-2,6-diyl-*alt*-(4,7-bis(2-thienyl)-2,1,3-benzothiadiazole)-5,5′-diyl] (Si-PCPDTBT), yielding a certified efficiency of 5.24% with a doctor-bladed active layer [22], but a significantly lower efficiency of 0.64% when used in inkjet trials [6], primarily attributed to the low current density as well as fill factor achieved. This conjugated polymer is particularly interesting as it has a low bandgap of approx. 1.7 eV and therefore absorbs across a wide wavelength range around 700 nm [22]. This makes it a worthwhile candidate for several organic solar cell applications, including tandem cells [23]. The second conjugated polymer included in this study is poly[*N*-9″-hepta-decanyl-2,7-carbazole-alt-5,5-(4′,7′-di-2-thienyl-2′,1′,3′-benzothiadiazole)] (PCDTBT), which has been shown to achieve a power conversion efficiency of approx. 7% and high IQE values approaching 100% [24]. This conjugated polymer has so far not been utilised in studies involving inkjet printing.

In this paper we discuss the processing conditions to fabricate efficient BHJ organic solar cells based on inkjet-printed active layers using the materials shown in Fig. 1. By employing current/voltage, atomic force microscopy, photoluminescence quenching and external/internal quantum efficiency techniques we discuss the results in relation to doctor-bladed reference devices.

2. Experimental details

The organic solar cells were deposited on pre-patterned indium tin oxide (ITO) substrates (Psiotec, UK) using a normal device architecture. First, a ~50 nm hole transporting layer of Clevios PH poly(3,4-ethylenedioxylthiophene):poly(styrenesulfonate) (PEDOT:PSS) (1:3.2 by volume with isopropanol) was deposited using a doctor blade (Erichsen, Germany) and annealed for 20 min at 140 °C in air. On top of this the active layers consisting of, respectively, Si-PCPDTBT:$PC_{71}BM$ (1:1.5 by weight) and PCDTBT:$PC_{71}BM$ (1:2 by weight) were doctor-bladed (for the reference devices) or inkjet-printed using a commercially available printer fitted with a piezo-driven 16-nozzle printhead with integrated reservoir and a nominal drop volume of 10 pl (Fujifilm Dimatix, USA). Both inkjet-printed and doctor-bladed active layers were dried in air by remaining on the heated surface until visible solvent evaporation had occurred. In a final step, ~20 nm calcium and ~100 nm aluminium were evaporated under vacuum at a chamber base pressure of 10^{-6} mbar. The finished devices were encapsulated under a cover glass (Ossila, UK) using UV-activated adhesive (Dymax, USA). All components of the organic solar cells, except for the final metal evaporation step and encapsulation, were handled and deposited in air. Over 100 cells were produced for this study, each with an active device area of 9 mm^2, accurately defined by the shadow mask used for evaporating the top electrode.

Si-PCPDTBT was purchased from Konarka, Germany, PCDTBT from 1-material, Canada, $PC_{70}BM$ from Solenne, The Netherlands, and Clevios PH PEDOT:PSS from Heraeus, Germany. Uniform layer thicknesses were measured using a Dektak 150 step profilometer (Veeco, USA). Atomic force microscopy to analyse layer surface roughness and morphology was carried out in tapping mode using an Easyscan 2 system (Nanosurf, Switzerland). Device parameters and current/voltage characteristics were obtained using a source-meter (Keithley, USA) and solar simulator calibrated to 100 mW/cm^2 light intensity (Newport, USA). External quantum efficiency (EQE) measurements were performed on a setup comprising a monochromated light source originating from a xenon lamp, a mechanical chopper, a preamplifier and a lock-in amplifier (Newport Oriel, USA).

Internal quantum efficiency (IQE) was calculated by dividing the external quantum efficiency of each cell under study by the absorption spectra of the corresponding active layer. The absorption spectra have been calculated using the transfer-matrix formalism [25] in a MATLAB script provided by Ref. [26] based on our OPV device stack of glass/ITO/PEDOT/active layer/Ca/Al. The refractive index n and extinction coefficient k in our polymer:fullerene systems was $n=2$ and $k=\lambda a/4\pi$ (with λ the wavelength and a the absorption coefficient in our active layer) as per Ref. [26]. Good agreement is seen between the calculated k values and those experimentally obtained using ellipsometry [27,28].

Steady-state photoluminescence (PL) was performed using a 0.75 m spectrometer equipped with a charge-coupled device (CCD) camera with spectral response up to 1100 nm. The PL was quasi-resonantly excited by a continuous wave (cw), power-stabilized He–Ne laser at 632 nm, operated at moderate excitation densities of ~15 mW/cm^2. All PL data were acquired with samples placed in vacuum conditions (ca. 10^{-5} mbar). The PL quenching measurements were performed on a side-by-side sample geometry to allow a direct intensity comparison. The emission of each film was normalized to its optical absorbance (optical density) to take into account film thickness and concentration variations. All PL spectra were corrected for the instrument response at the detection range.

3. Results and discussion

An inkjet printer, while providing several advantages such as drop-on-demand technology, therefore using minimal material quantities, requires careful adjusting of the processing conditions to allow fabrication of smooth films. Due to the inkjet printing process taking place line by line, it is important that the active

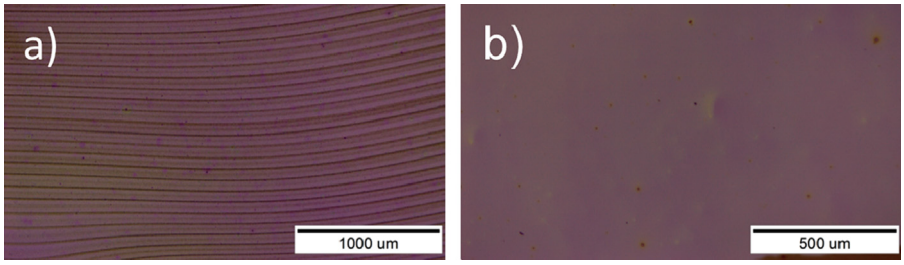

Fig. 2. Optical micrographs of inkjet-printed Si-PCPDTBT:$PC_{70}BM$ blend films. Initially in (a) lines are clearly visible, while in (b) after control of the printing processing parameters smooth films are obtained.

layer solution forms a homogenous film on the substrate. This is achieved by each printed line merging in just the right way with the previous and next printed line.

Early on in our study inhomogeneous films were produced. This led to poor solar cell device performance as generated charges did not have uninterrupted pathways to the electrodes (see Fig. 2a). This was reflected in the obtained solar cell performance parameters, which gave very low current density values (not shown here).

The parameters that were controlled during the inkjet printing process to improve the merging behaviour are the drop spacing parameter (the distance between each deposited droplet of solution), the substrate temperature and the ink properties itself, specifically the concentration and choice of solvent. These parameters together influence the drying behaviour of the film. Higher boiling point solvents provide slower evaporation rates, thereby allowing longer drying times and giving the molecules more time to arrange in the most energy-stable conformation, whereas lower-boiling solvents can induce an order of crystallinity that is not favourable [29,30].

These parameters can be influenced by increasing the substrate temperature and manipulating the molecular ordering. Ideally, the drying behaviour of the inkjet-printed films mimics the drying behaviour of the reference doctor-bladed layers. Further detailed descriptions regarding droplet formation and drying effects, such as Marangoni flow, are given elsewhere [31–33].

In our case, the solution properties were particularly important to allow the cartridge to successfully eject the solution. As will be described in detail below, this was achieved by choosing the appropriate concentration in the case of Si-PCPDTBT:$PC_{70}BM$ active layer and choosing the appropriate solvent in the case of PCDTBT:$PC_{70}BM$-based devices. The resulting smooth films can be seen in Fig. 2b of the optical micrographs of representative inkjet-printed Si-PCPDTBT:$PC_{70}BM$ layers.

3.1. Processing conditions for inkjet-printed PCDTBT:$PC_{70}BM$ and Si-PCPDTBT:$PC_{70}BM$ active layers

3.1.1. Inkjet-printed PCDTBT:$PC_{70}BM$ OPVs

This is the first report of inkjet-printing processing parameters for PCDTBT. The starting point for the use of PCDTBT:$PC_{70}BM$ in inkjet-printed active layers is the choice of solvent. From previous work we know that using a high boiling point (b.p.) solvent is crucial to allow the droplets to be ejected from the cartridge [17,21]. Low boiling point solvents can lead to nozzle clogging or nozzle misfiring and even prevent solution from being ejected altogether.

For the doctor-bladed reference devices chlorobenzene was used as a solvent and device performance parameters of 888 mV, 10.3 mA/cm^2, 53.7% and 4.91% for V_{oc}, J_{sc}, FF and PCE, respectively, were achieved. While these values represent the highest efficiency obtained for PCDTBT:$PC_{70}BM$ using doctor-blading, we replaced the chlorobenzene (CB, b.p. 131 °C) [34] used for the reference device with ortho-dichlorobenzene (oDCB, b.p. 181 °C) [34] to enable reproducible printing and inkjet-printed the active layer material using various drop-spacing values at a platen temperature of 40 °C and an ink temperature of 60 °C. As previously reported for inkjet-printed active layers using oDCB as a solvent, these respective temperature regions lead to optimum solvent evaporation and therefore drying behaviour of the small amounts of solution that are ejected onto the substrate line by line as well as appropriate solution viscosity within the cartridge to avoid nozzle clogging [17].

Initially, when increasing the drop-spacing of the inkjet nozzles the device efficiencies improve. This is primarily due to an increase in fill factor (FF) and short-circuit current density (J_{sc}), which compensates for the small loss in open-circuit voltage (V_{oc}).

When the drop-spacing parameter is increased, the film becomes thinner—from approximately 100 nm at DS40 to approximately 70 nm at DS46. This would normally lead to a decrease in absorption strength, as fewer photons are able to be absorbed, and thereby lead to a reduction in achievable photocurrent density. However, the fill factor increase indicates that charge collection at the electrodes is improved with a thinner layer, so much so that overall a higher current density is produced from the available electrons. At DS46 this trade-off seems to have reached its limit as the fill factor continues to increase, however the current decreases, leading to a worse PCE overall. The best overall device efficiency using an inkjet-printed active layer was ~3.9% and was achieved for a drop-spacing parameter of 44 μm (DS44).

To obtain an understanding of this drop in performance when compared to the reference devices doctor-bladed from CB, we fabricated solar cells by doctor-blade using oDCB, i.e. the same solvent used for inkjet printing, using a substrate temperature of 95 °C (70 °C for CB). This resulted in device performance parameters of 833 mV, 10.6 mA/cm^2, 44.1% and 3.89% for V_{oc}, J_{sc}, FF and PCE, respectively, indicating comparable results for inkjet-printed and doctor-bladed active layers using oDCB as a solvent. The slight difference in J_{sc} and FF between the doctor-bladed and inkjet-printed device performance may be explained by a slight variation in thickness (as shown in Table 1). This may result in the higher J_{sc} seen in the case of the slightly thicker doctor-bladed film. However, the FF decrease for the same device may indicate some morphological limitations.

All the achieved device parameters and J/V characteristics using PCDTBT:$PC_{70}BM$ active layers are summarised in Table 1 and shown in Fig. 3, respectively. While the best reference devices fabricated from CB produced approx. 5% efficient solar cells, the doctor-bladed devices fabricated from oDCB showed equal efficiencies of approx. 4% to inkjet-printed solar cells fabricated from oDCB. This indicates the set of processing conditions used for inkjet-printing are able to control the PCDTBT:$PC_{70}BM$ system to produce efficient organic solar cells.

3.1.2. Inkjet-printed Si-PCPDTBT:$PC_{70}BM$ OPVs

In the case of Si-PCPDTBT, we obtain a significant increase in device performance compared to previously reported devices using an inkjet-printed active layer of this material [6]. This

Table 1
Overview of device performance parameters of all solar cells with active layers deposited using inkjet printing (IJ) with various drop-spacing (DS), and by doctor-blading (DB). The reference device performance is shown in italics, while the best achieved inkjet-printed device performance is shown in bold.

Active layer	Solvent	Concentration [mg/ml]	Film thickness [nm]	Process	V_{oc} [mV]	J_{sc} [mA/cm^2]	FF [%]	PCE [%]
PCDTBT: $PC_{70}BM$	oDCB	15	~100	IJ DS40	864	8.2	41.3	2.95
			~90	IJ DS42	859	8.5	43.3	3.20
			~80	**IJ DS44**	**834**	**9.7**	**47.8**	**3.86**
			~70	IJ DS46	824	9.4	48.6	3.76
			~90	DB	833	10.6	44.1	3.89
	CB		*~90*	*DB*	*888*	*10.3*	*53.7*	*4.91*
Si-PCPDTBT: $PC_{70}BM$	oDCB	12.5	~120	IJ DS35	658	5.5	42.1	1.53
			~90	**IJ DS40**	**661**	**8.1**	**56.2**	**3.01**
			~80	IJ DS42	647	6.7	52.8	2.28
			~100	*DB*	*610*	*16.8*	*55.2*	*5.66*
		25	~110	DB	630	15.5	56.3	5.45

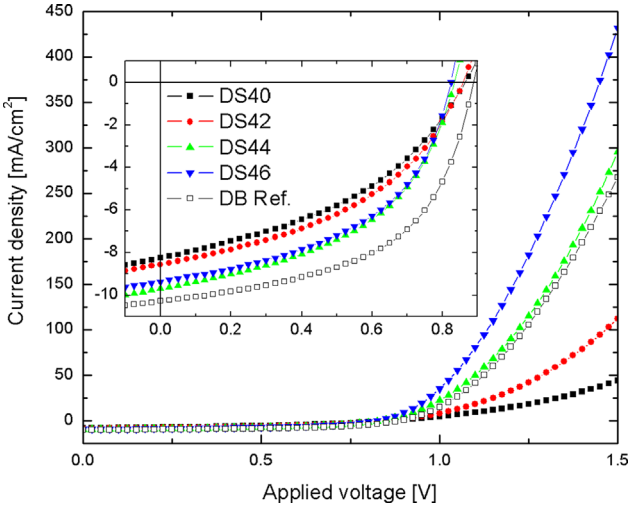

Fig. 3. *J*/*V* characteristics of OPVs using inkjet-printed PCDTBT:$PC_{70}BM$ active layers.

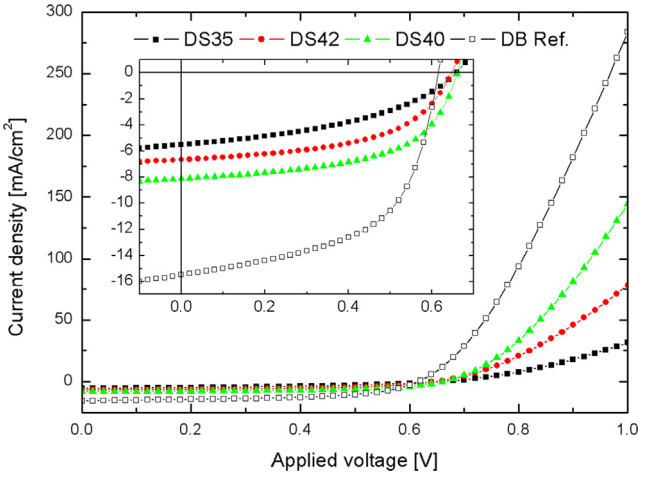

Fig. 4. *J*/*V* characteristics of OPVs using inkjet-printed Si-PCPDTBT:$PC_{70}BM$ active layers.

improvement is predominantly attributed to better control of the active layer morphology.

The solvent used for Si-PCPDTBT is the same for both reference and inkjet-printed systems as poor solubility prevents lower boiling point solvents being used in the first place. For the doctor-bladed reference devices an initial concentration of 25 mg/ml was used and device performance parameters of 630 mV, 15.5 mA/cm^2, 56.3% and 5.45% for V_{oc}, J_{sc}, FF and PCE, respectively, were achieved.

However, inkjet-printed active layers of Si-PCPDTBT:$PC_{70}BM$ initially showed low device performance values in the range of 1.5% using oDCB at the reference concentration of 25 mg/ml. The V_{oc} values were better than the reference device with values up to 650 mV, but current density and fill factor were far below optimum with only approximately 5 mA/cm^2 and 44%, respectively (not shown here). As the printing process at this stage was continuously hampered by the inkjet cartridge not ejecting droplets continuously, the concentration of solute to solvent was halved to 12.5 mg/ml while retaining the same conjugated polymer:fullerene ratio in order to increase the flow through the nozzles.

This then became the new reference concentration, since doctor-bladed device efficiencies using the lower concentration of 12.5 mg/ml yielded slightly improved device performance parameters of 610 mV, 16.8 mA/cm^2, 55.2% and 5.66% for V_{oc}, J_{sc}, FF and PCE, respectively. Additionally, this new suggested concentration yields the highest OPV efficiency using Si-PCPDTBT:$PC_{70}BM$ in the literature.

The inkjet-printed active layers using the new concentration showed similar behaviours to the active layer blend of PCDTBT:$PC_{70}BM$, in that the thickness of the active layer decreases with increasing drop-spacing—from approximately 120 nm at DS35 to approximately 80 nm at DS42. Again, although a thinner active layer is present, improved FF values indicate improved collection of the created charges at the electrodes, explaining the large increases in all device performance parameters that result in a doubling of PCE from devices fabricated with an inkjet-printed active layer using DS35 to ones using DS40.

Overall, a 3% efficient OPV device was fabricated using DS40 parameter at 40 °C substrate temperature, as summarised in the device performance parameters and *J*/*V* characteristics in Table 1 and Fig. 4. Due to the fact that as opposed to the PCDTBT:$PC_{70}BM$ system, the Si-PCPDTBT:$PC_{70}BM$ shows a significant difference in the achieved device performance of doctor-bladed and inkjet-printed solar cells, the following section will examine the origins of this difference of the active layer morphology using atomic force microscopy, photoluminescence quenching and external quantum efficiency techniques.

3.2. Analysis of inkjet-printed active layer morphology and device performance

Atomic force microscopy (AFM) was used to obtain images showing structuring of the blend film of the inkjet-printed active layers of both conjugated polymer blends with different drop-spacing settings (see Fig. 5). At higher drop-spacing the intermixing of conjugated polymer and $PC_{70}BM$ seems more homogenous, leading to improved device parameters as described previously.

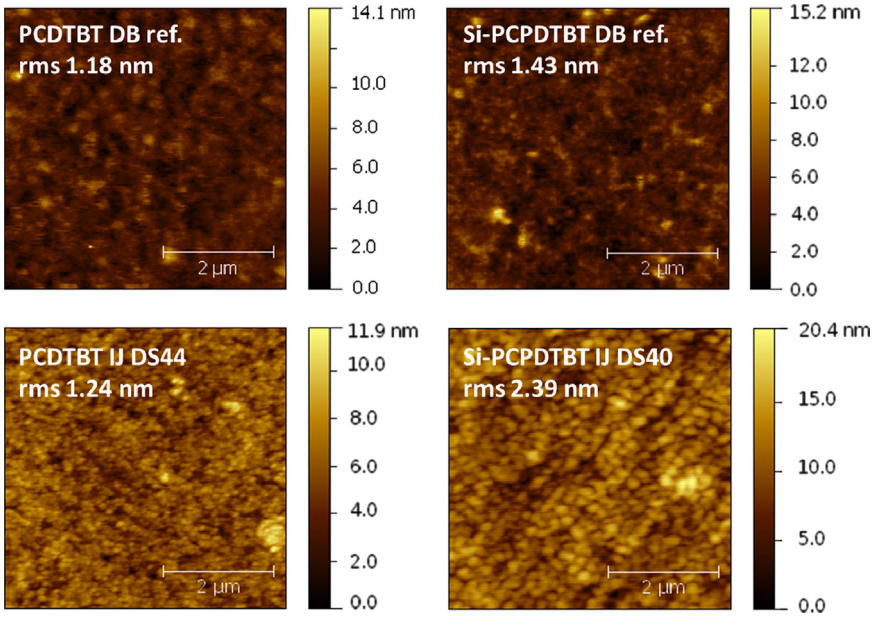

Fig. 5. AFM images of PCDTBT:$PC_{70}BM$ and Si-PCPDTBT:$PC_{70}BM$ active layers doctor-bladed (DB) and inkjet-printed (IJ) at DS40 and DS44, respectively. The scale bar represents 2 µm.

Additionally, the roughness values of inkjet-printed active layers with higher drop-spacing are closer to those observed in the doctor-bladed reference films, as seen in the PCDTBT:$PC_{70}BM$-based active layers.

The AFM images form the basis of the tentative interpretation why in the case of the Si-PCPDTBT:$PC_{70}BM$ blend devices the short circuit current density in the doctor-bladed reference devices shows approximately double the value as the inkjet-printed devices. The inkjet-printed active layer seems to show more pronounced areas than the doctor-bladed film's more intermixed, less well defined structure. These more pronounced areas could be viewed as a morphology with larger feature sizes or domains. These yield fewer electrons available overall in the active layer as there is a lower dissociation area of generated excitons. However, these domains can provide potentially better transport to the electrodes as they are better connected, leading to higher fill factors, but potentially lower current, as we observe in our devices. Inversely, the enhanced dissociation and resulting photocurrent in the doctor-bladed films can be attributed to the smaller feature sizes [35].

In order to confirm the influence of these features on the overall generated current, photoluminescence (PL) quenching measurements were carried out. The degree of PL quenching is an indicator to evaluate the charge separation efficiency in donor/acceptor blend films [36].

Comparative normalized PL spectra of Si-PCPDTBT and Si-PCPDTBT:$PC_{70}BM$ films produced with the two aforementioned deposition techniques, are displayed in Fig. 6. The pristine polymer emission is dominated in both cases by a vibronic peak at ~800 nm, while a weaker, lower energy vibronic is visible at ~920 nm. The blend PL appears broader due to the contribution of the PCBM emission peaked at ~716 nm [37]. The small, reproducible blue shift (~12 meV) in the polymer emission from the blends compared to the pristine PL energy can be attributed to dielectric screening effects due to the PCBM material. As expected, the PL intensity of the blend films appears quenched compared to the respective pristine films emission. The steady-state emission quenching R yields a measure of the interfacial polymer exciton dissociation efficiency and can be quantified by the following ratio:

$$R\ [\%] = \frac{I_{pristine} - I_{blend}}{I_{pristine}} \times 100\%, \quad (1)$$

where $I_{pristine}$ and I_{blend} are the integrated PL emission from pristine and blend films, respectively. From Fig. 6 it is evident that PL quenching of the doctor-bladed films appears significantly more efficient to that of inkjet-printed films. The results are in agreement with the AFM findings, i.e. the presence of larger features in the microstructure of the inkjet-printed films. The larger domains limit the efficiency of exciton diffusion and interfacial dissociation and thus the charge extraction yield in the inkjet-printed solar cells, resulting in reduced photocurrents compared to the doctor-bladed devices.

Finally, the external (and internal) quantum efficiency of reference and inkjet-printed devices shows the efficiency of incident (and absorbed) photon to electron conversion, as depicted in Fig. 7. The inkjet-printed devices have worse EQE in the case of both conjugated polymers, which was to be expected since in both cases the J_{sc} is also lower when compared to the reference devices. However, the results show that the offset is larger for Si-PCPDTBT:$PC_{70}BM$ devices as opposed to PCDTBT:$PC_{70}BM$ ones. The EQE observations are in good agreements with the morphological limitations of inkjet-printed devices described in detail above.

In order to suppress the influence of absorption, the IQE was determined for both polymer systems. The calculated absorption spectra and resulting IQE are only given at wavelengths at which the polymer absorbs, since the error of the calculation increases outside the absorption limits [26].

Overall, as with EQE, the doctor-bladed devices provide better conversion of the absorbed photons to electrons compared with the corresponding inkjet printed devices. In the case of the PCDTBT system, the difference between the inkjet-printed and doctor-bladed IQE is only slight, indicating that the absorbed photons are converted to electrons similarly efficiently. For the Si-PCPDTBT system, the difference between inkjet-printed and doctor-bladed devices is more pronounced, indicating less efficient photon to electron conversion.

Since the IQE only takes into account photons that have been absorbed and since the device electrodes are the same for both the inkjet-printed and doctor-bladed systems, we assume this difference in IQE stems from the morphological limitations within the active layer. This is in line with the previous observations from AFM and photoluminescence measurements and shows the limitations that

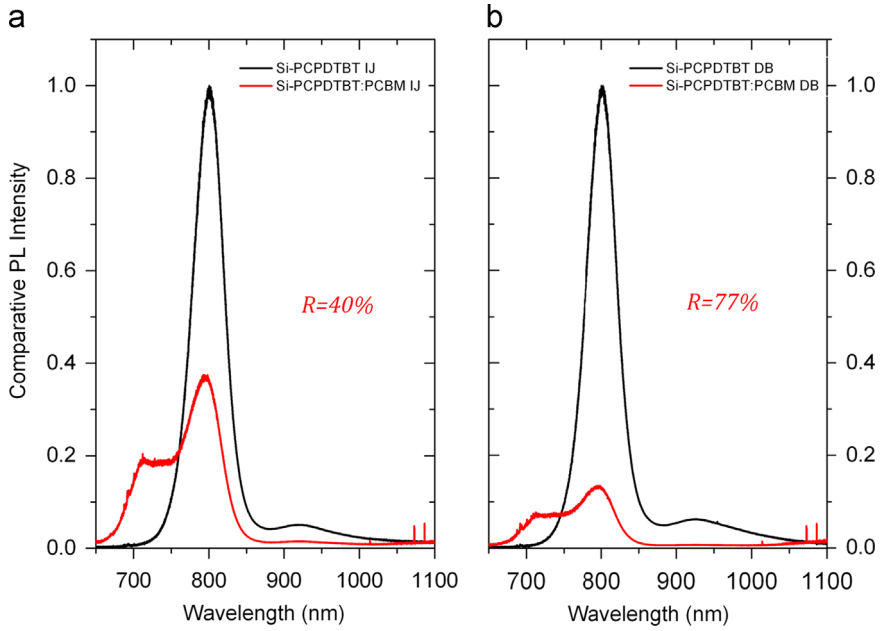

Fig. 6. Comparative PL spectra of inkjet-printed (IJ, (a)) and doctor-bladed (DB, (b)) Si-PCPDTBT pristine and Si-PCPDTBT:$PC_{70}BM$ blend films. The spectra have been normalized to the emission of the pristine film in each case.

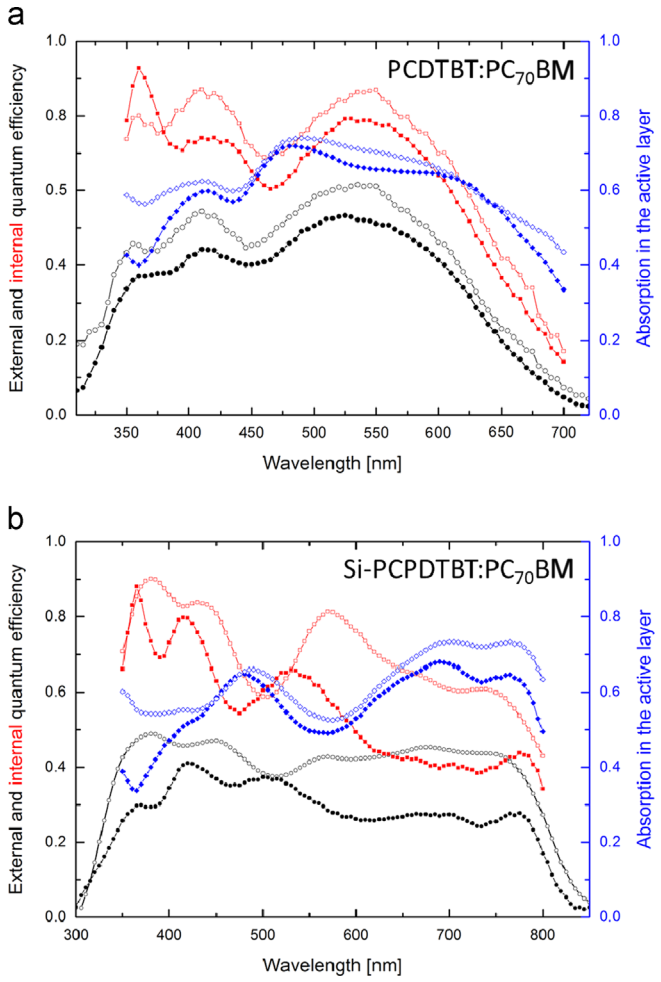

Fig. 7. Measured EQE (black circles), calculated absorption (blue diamonds) and calculated IQE (red squares) in solar cells with (a) PCDTBT:$PC_{70}BM$ and (b) Si-PCPDTBT:$PC_{70}BM$ active layers. Open symbols represent doctor-bladed and filled symbols inkjet-printed active layers. (For interpretation of the references to color in this figure legend, the reader is referred to the web version of this article.)

need to be overcome in order for inkjet-printed active layers to provide equally good IQE as doctor-bladed films.

4. Conclusion

We have presented efficient organic solar cells using inkjet-printed active layers of Si-PCPDTBT:$PC_{70}BM$ and PCDTBT:$PC_{70}BM$ blends of ~3% and ~4% power conversion efficiency, respectively. We have presented the processing parameters and described routes to overcoming the inkjet processing problems of film formation, i.e. line merging and of nozzle clogging, by using appropriate solvents and blend concentrations. In the case of Si-PCPDTBT:$PC_{70}BM$ blends the concentration needed to initially be halved in order to print efficiently, while in the case of PCDTBT:$PC_{70}BM$ blends the concentration remained the same, however the solvent needed to be changed in order for effective printing.

While for the PCDTBT:$PC_{70}BM$ system the primary reason for the lower device performance using inkjet-printed active layers can be attributed to the change in solvent, for the Si-PCPDTBT:$PC_{70}BM$ system the lower device performance seems to stem from a difference in the morphology within the active layers when fabricated with the two different techniques. This yields lower exciton dissociation efficiency and ultimately lower photogenerated current as shown by PL quenching.

Despite the limitations on the short-circuit current density for the inkjet-printed OPVs of the Si-PCPDTBT blend when compared to reference OPVs fabricated by doctor blade, the resulting power conversion efficiencies are the highest in the literature using inkjet-printing as a deposition technique for both conjugated polymer material systems presented herein.

Acknowledgements

This work was co-funded by the European Regional Development Fund and the Republic of Cyprus through the Research Promotion Foundation (Strategic Infrastructure Project NEA ΥΠΟΔΟΜΗ/ΣΤΡΑΤΗ/0308/06). We would like to thank Dr Marios Neophytou for numerous fruitful discussions.

References

[1] United States Department of Energy, Office of Science, Basic Research Needs for Solar Energy Utilization, Argonne National Laboratory, Lemont, IL, 2005.
[2] Z. He, C. Zhong, X. Huang, W.-Y. Wong, H. Wu, L. Chen, S. Su, Y. Cao, Simultaneous enhancement of open-circuit voltage, short-circuit current density, and fill factor in polymer solar cells, Adv. Mater. 23 (2011) 4636.
[3] M.A. Green, K. Emery, Y. Hishikawa, W. Warta, E.D. Dunlop, Solar cell efficiency tables (version 41), Prog. Photovoltaics Res. Appl. 21 (2013) 1.
[4] T.D. Nielsen, C. Cruickshank, S. Foged, J. Thorsen, F.C. Krebs, Business, market and intellectual property analysis of polymer solar cells, Sol. Energy Mater. Sol. Cells 94 (2010) 1553.
[5] J.X. Zhou, J.Y.H. Fuh, H.T. Loh, Y.S. Wong, Y.S. Ng, J.J. Gray, S.J. Chua, Characterization of drop-on-demand microdroplet printing, Int. J. Adv. Manuf. Technol. 48 (2009) 243.
[6] A. Teichler, R. Eckardt, S. Hoeppener, C. Friebe, J. Perelaer, A. Senes, M. Morana, C.J. Brabec, U.S. Schubert, Combinatorial screening of polymer:fullerene blends for organic solar cells by inkjet printing, Adv. Energy Mater. 1 (2010) 105.
[7] A. Teichler, J. Perelaer, U.S. Schubert, Inkjet printing of organic electronics—comparison of deposition techniques and state-of-the-art developments, J. Mater. Chem. C 1 (2013) 1910.
[8] A. Teichler, J. Perelaer, F. Kretschmer, M.D. Hager, U.S. Schubert, Systematic investigation of a novel low-bandgap terpolymer library via inkjet printing: influence of ink properties and processing conditions, Macromol. Chem. Phys. 214 (2013) 664.
[9] A. Teichler, J. Perelaer, U.S. Schubert, Screening of film-formation qualities of various solvent systems for π-conjugated polymers via combinatorial inkjet printing, Macromol. Chem. Phys. 214 (2013) 547.
[10] R.R. Søndergaard, M. Hösel, F.C. Krebs, Roll-to-roll fabrication of large area functional organic materials, J. Polym. Sci., Part B: Polym. Phys. 51 (2013) 16.
[11] M. Hösel, R.R. Søndergaard, D. Angmo, F.C. Krebs, Comparison of fast roll-to-roll flexographic, inkjet, flatbed, and rotary screen printing of metal back electrodes for polymer solar cells, Adv. Eng. Mater. 15 (2013) 995.
[12] D. Angmo, J. Sweelssen, R. Andriessen, Y. Galagan, F.C. Krebs, Inkjet printing of back electrodes for inverted polymer solar cells, Adv. Energy Mater. 3 (2013) 1230.
[13] D. Angmo, T.T. Larsen-Olsen, M. Jørgensen, R.R. Søndergaard, F.C. Krebs, Roll-to-roll inkjet printing and photonic sintering of electrodes for ITO free polymer solar cell modules and facile product integration, Adv. Energy Mater. 3 (2013) 172.
[14] C.N. Hoth, S.A. Choulis, P. Schilinsky, C.J. Brabec, High photovoltaic performance of inkjet printed polymer:fullerene blends, Adv. Mater. 19 (2007) 3973.
[15] Y. Galagan, J.-E.J.M. Rubingh, R. Andriessen, C.-C. Fan, P.W.M. Blom, S.C. Veenstra, J.M. Kroon, ITO-free flexible organic solar cells with printed current collecting grids, Sol. Energy Mater. Sol. Cells 95 (2011)1339 95 (2011).
[16] M. Neophytou, F. Hermerschmidt, A. Savva, E. Georgiou, S.A. Choulis, Highly efficient indium tin oxide-free organic photovoltaics using inkjet-printed silver nanoparticle current collecting grids, Appl. Phys. Lett. 101 (2012) 193302.
[17] M. Neophytou, W. Cambarau, F. Hermerschmidt, C. Waldauf, C. Christodoulou, R. Pacios, S.A. Choulis, Inkjet-printed polymer–fullerene blends for organic electronic applications, Microelectron. Eng. 95 (2012) 102.
[18] A. Lange, A. Hollaender, M. Wegener, Modified processing conditions for optimized organic solar cells with inkjet printed P3HT:PC61BM active layers, Mater. Sci. Eng., B 178 (2013) 299.
[19] S.H. Eom, H. Park, S.H. Mujawar, S.C. Yoon, S.-S. Kim, S.-I. Na, S.-J. Kang, D. Khim, D.-Y. Kim, S.-H. Lee, High efficiency polymer solar cells via sequential inkjet-printing of PEDOT:PSS and P3HT:PCBM inks with additives, Org. Electron. 11 (2010) 1516.
[20] A. Lange, W. Schindler, M. Wegener, K. Fostiropoulos, S. Janietz, Inkjet printed solar cell active layers prepared from chlorine-free solvent systems, Sol. Energy Mater. Sol. Cells 109 (2013) 104.
[21] C.N. Hoth, P. Schilinsky, S.A. Choulis, C.J. Brabec, Printing highly efficient organic solar cells, Nano Lett. 8 (2008) 2806.
[22] M.C. Scharber, M. Koppe, J. Gao, F. Cordella, M.A. Loi, P. Denk, M. Morana, H.-J. Egelhaaf, K. Forberich, G. Dennler, R. Gaudiana, D. Waller, Z. Zhu, X. Shi, C.J. Brabec, Influence of the bridging atom on the performance of a low-bandgap bulk heterojunction solar cell, Adv. Mater. 22 (2010) 367.
[23] C.-H. Chou, W.L. Kwan, Z. Hong, L.-M. Chen, Y. Yang, A metal-oxide interconnection layer for polymer tandem solar cells with an inverted architecture, Adv. Mater. 23 (2011) 1282.
[24] S.H. Park, A. Roy, S. Beaupré, S. Cho, N. Coates, J.S. Moon, D. Moses, M. Leclerc, K. Lee, A.J. Heeger, Bulk heterojunction solar cells with internal quantum efficiency approaching 100%, Nat. Photonics 3 (2009) 297.
[25] L.A.A. Pettersson, L.S. Roman, O. Inganäs, Modeling photocurrent action spectra of photovoltaic devices based on organic thin films, J. Appl. Phys. 86 (1999) 487.
[26] G.F. Burkhard, E.T. Hoke, M.D. McGehee, Accounting for interference, scattering, and electrode absorption to make accurate internal quantum efficiency measurements in organic and other thin solar cells, Adv. Mater. 22 (2010) 3293.
[27] H. Azimi, M. Morana, T. Ameri, B. Dastmalchi, M.C. Scharber, K. Hingerl, C.J. Brabec, Determining the internal quantum efficiency of organic bulk heterojunctions based on mono and bis—adduct fullerenes as acceptor, Sol. Energy Mater. Sol. Cells 95 (2011) 3093.
[28] C. Cho, J.-Y. Lee, Multi-scale and angular analysis of ray-optical light trapping schemes in thin-film solar cells: micro lens array, V-shaped configuration, and double parabolic trapper, Opt. Express 21 (2013) A276.
[29] Y.-S. Kim, Y. Lee, J.K. Kim, E.-O. Seo, E.-W. Lee, W. Lee, S.-H. Han, S.-H. Lee, Effect of solvents on the performance and morphology of polymer photovoltaic devices, Curr. Appl. Phys. 10 (2010) 985.
[30] G. Li, V. Shrotriya, J. Huang, Y. Yao, T. Moriarty, K. Emery, Y. Yang, High-efficiency solution processable polymer photovoltaic cells by self-organization of polymer blends, Nat. Mater. 4 (2005) 864.
[31] H. Hu, R.G. Larson, Marangoni effect reverses coffee-ring depositions, J. Phys. Chem. B 110 (2006) 7090.
[32] D. Soltman, V. Subramanian, Inkjet-printed line morphologies and temperature control of the coffee ring effect, Langmuir 24 (2008) 2224.
[33] M. Layani, M. Gruchko, O. Milo, I. Balberg, D. Azulay, S. Magdassi, Transparent conductive coatings by printing coffee ring arrays obtained at room temperature, ACS Nano 3 (2009) 3537.
[34] D.R. Lide (Ed.), CRC Handbook of Chemistry and Physics, CRC Press, Boca Raton, FL, 2005.
[35] E.L. Williams, S. Gorelik, I. Phang, M. Bosman, C. Vijila, G.S. Subramanian, P. Sonar, J. Hobley, S.P. Singh, H. Matsuzaki, A. Furube, R. Katoh, Nanoscale phase domain structure and associated device performance of organic solar cells based on a diketopyrrolopyrrole polymer, RSC Adv. 3 (2013) 20113.
[36] T.E. Kang, H.-H. Cho, C.-H. Cho, K.-H. Kim, H. Kang, M. Lee, S. Lee, B. Kim, C. Im, B.J. Kim, Photoinduced charge transfer in donor–acceptor (DA) copolymer: fullerene bis-adduct polymer solar cells, ACS Appl. Mater. Interfaces 5 (2013) 861.
[37] A. Othonos, G. Itskos, M. Neophytou, S.A. Choulis, Excitation dynamics of a low bandgap silicon-bridged dithiophene copolymer and its composites with fullerenes, Appl. Phys. Lett. 100 (2012) 153303.